Available online at www.sciencedirect.com
SCIENCE DIRECT®
Journal of Catalysis 224 (2004) 404–416
JOURNAL OF CATALYSIS
www.elsevier.com/locate/jcat

Behavior of active sites on Cr-MCM-41 catalysts during the dehydrogenation of propane with CO_2

Katsuomi Takehira,[a,*] Yoshihiko Ohishi,[a] Tetsuya Shishido,[b] Tomonori Kawabata,[a] Ken Takaki,[a] Qinghong Zhang,[c] and Ye Wang [c]

[a] *Department of Chemistry and Chemical Engineering, Graduate School of Engineering, Hiroshima University, Kagamiyama 1-4-1, Higashi-Hiroshima 739-8527, Japan*

[b] *Department of Chemistry, Tokyo Gakugei University, Nukui-kita 4-1-1, Koganei, Tokyo 184-8501, Japan*

[c] *State Key Laboratory for Physical Chemistry of Solid Surfaces, Department of Chemistry, Xiamen University, Xiamen 361005, China*

Received 8 December 2003; revised 3 March 2004; accepted 4 March 2004

Available online 20 April 2004

Abstract

M-MCM-41 catalysts (M: V, Cr, Mn, Fe, Co, Ni, and Ga) prepared by direct hydrothermal (DHT) synthesis have been tested for dehydrogenation of propane with carbon dioxide. The synthesized materials were characterized by X-ray diffraction (XRD), N_2 adsorption (77 K), diffuse reflectance UV–vis, UV-Raman, and X-ray absorption (XANES and EXAFS) spectroscopic measurements. Cr-MCM-41 showed the highest activity among M-MCM-41 catalysts tested, resulting in the production of propene with a conversion of 30% and a selectivity above 90%. The rate of carbon monoxide formation increased together with that of propene, while the rate of hydrogen formation stayed at almost constant value, with increasing the partial pressure of carbon dioxide. The mechanism of catalyst deactivation as well as regeneration was discussed based on the structure–catalytic property relationships. It is suggested that Cr(VI) in tetrahedral coordination formed as an active monochromate species and reduced to Cr(III) in octahedral coordination as a less active polychromate species during the reaction. Deactivated catalyst was regenerated by a treatment with gaseous oxygen, during which a reoxidation of the Cr(III) species to the Cr(VI) species was observed. Not only oxygen but also carbon dioxide could regenerate $Cr(VI)O_4$ tetrahedra from reduced $Cr(III)O_6$ octahedra, even though the efficiency of carbon dioxide was lower than that of oxygen. It is concluded that during the reaction propane is dehydrogenated to propene by $Cr(IV)O_4$ tetrahedra, which is simultaneously reduced to $Cr(III)O_6$ octahedra. The reduced $Cr(III)O_6$ octahedra can be reoxidized to $Cr(VI)O_4$ tetrahedra by carbon dioxide, and thus the reduction–oxidation cycle between $Cr(VI)O_4$ tetrahedra and $Cr(III)O_8$ octahedra has an important role in the dehydrogenation of propane with carbon dioxide over Cr-MCM-41.

Keywords: Cr-MCM-41; Chromate species; Carbon dioxide; Dehydrogenation; Propane; Deactivation; Regeneration

1. Introduction

Catalytic conversions of alkanes into the corresponding alkenes are of increasing importance because of the growing demand for alkenes. Chromium-based catalysts have received much attention because of their wide use in many catalytic reactions [1,2]. Silica- and alumina-supported chromium oxides were industrially used for the productions of lower alkenes such as ethene, propene, and isobutene through the dehydrogenation of the corresponding alkanes [3,4]. The reaction is endothermic and inevitably controlled by the thermodynamic equilibrium, requiring substantial energy consumption. Supported chromium oxides have also been investigated for the oxidative dehydrogenation of lower alkanes [5–11] or oxidation of other organic compounds with oxygen [12,13]. However, the use of oxygen as an oxidant is frequently accompanied by deep oxidation, resulting in a decrease in product selectivity.

Carbon dioxide as one of the major greenhouse gases has recently been considered as a source of carbon. Catalytic hydrogenation of carbon dioxide into several organic compounds has been intensively studied. In fact, carbon dioxide can also act as a mild oxidant and utilization of carbon dioxide in some partial oxidation reactions, such as CO_2 reforming of methane [14] and oxidative coupling of methane [15],

* Corresponding author. Fax: +81-(0)824-24-7744.
E-mail address: takehira@hiroshima-u.ac.jp (K. Takehira).

0021-9517/$ – see front matter
doi:10.1016/j.jcat.2004.03.014

has been reported. Carbon dioxide was found to enhance the dehydrogenation of ethane [16–18], propane [19–24], and isobutane [25] over supported chromium oxide. The reduction–oxidation property and the appropriate dispersion of chromium species on the support are important in these catalytic reactions [5,8].

MCM-41, a typical mesoporous molecular sieve, possesses uniform and well-ordered mesoporous channels with controllable pore sizes from 2 to 10 nm as well as a high surface area (ca. 1000 $m^2\ g^{-1}$) [26], and thus could be used as a promising catalyst support. Studies of chromium species introduced into MCM-41 would thus be useful in developing Cr-containing catalysts with desirable catalytic properties. There exist several studies on the synthesis and characterizations of Cr-MCM-41 [27–32]. For catalytic reactions, Cr-MCM-41 has been used for the liquid-phase oxidation with alkyl hydroperoxide [32,33] or hydrogen peroxide [34], but a leaching of chromium to the liquid phase is a big problem for the Cr-containing microporous and mesoporous materials [35–37]. Cr-MCM-41 prepared by an impregnation method was once used for the oxidative dehydrogenation of propane with oxygen, but the selectivity to propene was low and the yield to propene was lower than 5% [31]. Recently, a SBA-15-supported chromium oxide by the impregnation method has been applied to the dehydrogenation and the oxidative dehydrogenation of propane and showed good catalytic performance [38].

Recently, we applied two different methods, i.e., direct hydrothermal synthesis (DHT) and template-ion exchange (TIE), to the syntheses of V- [39], Fe- [40], and Mn-MCM-41 [41]. The two methods resulted in different locations and coordination environments of the incorporated metal cations, the TIE method provided highly dispersed metal ions on the wall surface of MCM-41 inside the mesopores, and the DHT method has a tendency to incorporate metal ions inside the framework of MCM-41. It has been clarified that the two different methods for introducing metal ions bring about remarkably different catalytic behavior in selective oxidation reactions. We have carefully studied the structures of Cr-MCM-41 prepared by direct hydrothermal synthesis and template-ion exchange by X-ray diffraction, N_2 adsorption, diffuse reflectance UV–vis, X-ray absorption (XANES and EXAFS), and UV-Raman spectroscopic measurements [42,43]. It was suggested that monochromate species mainly exist on the Cr-MCM-41 by the DHT method while several types of chromates species including both monochromates and polychromates coexist on that by the TIE method. In the dehydrogenation of propane over Cr-MCM-41-DHT, the selectivity to propene was higher than 90% with a yield of 30%, and the presence of carbon dioxide enhanced propane conversion. The chromate species on both types of samples are reduced to aggregated Cr(III) with octahedral coordination during the dehydrogenation reactions.

In the present paper, we report the deactivation behavior of Cr-MCM-41-DHT in the dehydrogenation of propane by carbon dioxide. The catalysts before and after the reaction are characterized in detail to obtain information about the change in structures and coordination environments of the introduced chromium species during the reaction. Moreover regeneration of the deactivated catalyst by oxygen or carbon dioxide is investigated and discussed to elucidate the structure–activity relationships for the Cr-MCM-41-DHT catalysts.

2. Experimental

2.1. Catalyst preparation

Various metals (M = Cr, Ga, Ni, V, Fe, Mn, and Co) were introduced into MCM-41 by direct hydrothermal synthesis. Metal nitrate, sodium silicate, and hexadecyltrimethylammonium bromide were used as the source of metal, silicone, and template, respectively. The molar ratio of the template to the silicone was kept at 0.5 in the synthesis gel for each synthesis. The synthesis gel was stirred for 1 h at room temperature and was then transferred to a Teflon bottle, which was placed in a stainless-steel autoclave after the adjustment of the pH value of the mixed gel to 10.5 with 4 M HCl. The hydrothermal synthesis was carried out at 150 °C for 48 h, and then the resultant solid was recovered by filtration, washed thoroughly with deionized water, and dried at 40 °C in vacuum for ca. 24 h. After calcination at 550 °C for 6 h in a flow of dry air, the M-MCM-41-DHT was obtained. Moreover Cr-MCM-41-DHT catalysts were prepared by changing the ratio of Cr to Si. Cr/Cab-O-Sil and Cr/SiO_2 catalysts were prepared by impregnation of nonporous Cab-O-Sil (M5, Acros Organics) and SiO_2 (JRC-SIO-8, the reference catalyst provided by the Catalyst Society of Japan) as a support for comparison with Cr(III) nitrate.

2.2. Characterizations of the catalysts

Inductively coupled plasma (ICP) optical emission spectroscopy was used for the determination of the metal content in each sample synthesized above. The measurements were performed with a Perkin-Elmer OPTIMA 3000, and the sample was dissolved in a mixture of HF and HNO_3 acids before the measurements.

N_2-adsorption studies were used to examine the porous properties of each sample. The measurements were carried out on Belsorp 18SP equipment (volumetric), and all the samples were pretreated in vacuum at 200 °C for 12 h before the measurements. The pore-size distribution was evaluated from the adsorption isotherm by the Dollimore and Heal (DH) method [44].

X-ray diffraction (XRD) patterns were collected on a SRA M18XHF diffractometer (MAC Science Co., Ltd., Japan) with Cu-Kα radiation (40 kV, 300 mA). Small divergent and scattering slits (0.05 mm) were selected to avoid a high background at low diffraction angles.

X-ray absorption spectroscopic measurements were performed with Synchrotron radiation at a beam-line BL7C

station of the Photon Factory, at the High Energy Accelerator Research Organization (Tsukuba, Japan), operated at 2.5 GeV with about 35–380 mA of ring current. The data were recorded in X-ray fluorescence mode at room temperature using a Si(111) double crystal monochromator. Energy was calibrated with Cu-K-edge absorption (8981.0 eV), and the energy step of measurement in the XANES region was 0.3 eV. The absorption was normalized to 1.0 at an energy position of 30 eV higher than the absorption edge. Data reductions were performed with the three FACOM M1800 computer system of the Data Processing Center of Kyoto University [45].

Diffuse reflectance UV–vis spectroscopic measurements were recorded on a Perkin-Elmer UV/VIS/NIR (Lambda 900) spectrometer. The spectra were collected at 200–700 nm referenced to $BaSO_4$. UV-Raman spectroscopic measurements were carried out with a Renishaw UV–vis Raman System 1000R using the UV line at 325 nm from a Kimmon IK 3201R-F He–Cd laser as the exciting source. The sample was loaded in an in situ cell and was treated in pure N_2 gas flow at 200 °C for dehydration before the measurement. A laser output of 30 mW was used and the maximum incident power at the sample was approximately 6 mW.

Temperature-programmed reduction (TPR) of the catalyst was performed at a heating rate of 10 °C min^{-1} from ambient temperature to 700 °C using a mixture of 5 vol% H_2/Ar as reducing gas after passing through a 13X molecular sieve trap to remove water. A U-shaped quartz tube reactor, the inner diameter of which was 6 mm, equipped with a TCD for monitoring the H_2 consumption was used. Prior to the TPR measurement, 50 mg of sample was calcined at 300 °C for 1 h in Ar gas flow at a rate of 20 ml min^{-1}.

Temperature-programmed oxidation (TPO) of the catalyst (0.2 g) after the reaction was performed at a heating rate of 2.5 °C min^{-1} using a mixture of 20 vol% O_2/N_2 as oxidizing gas. A U-shaped quartz tube reactor, the inner diameter of which was 6 mm, equipped with a TCD was used for monitoring the formation of CO_2. No other product than CO_2 was detected. The amount of coke formed on the catalyst during the reaction was calculated from the total amount of CO_2.

2.3. Catalytic reactions

The dehydrogenation of propane was carried out using a fixed-bed flow reactor at atmospheric pressure. A U-shaped quartz tube with an inner diameter of 4 mm was used as a reactor. In the dehydrogenation reactions, typically 0.4 g of catalyst, which had been pelletized and sieved to 250–417 μm in a diameter, was loaded into the reactor and treated in a gas flow containing N_2 (10 ml min^{-1}) and O_2 (10 ml min^{-1}) at 550 °C for 1 h and then purged with He (purity, 99.99%). The reaction was started by introducing a gas mixture of CO_2, C_3H_8, He, and N_2 to the reactor. N_2 was used as the internal standard for the calculations of the conversions of CO_2 and C_3H_8, while He was used for dilution to control the partial pressures of the reactants.

The products were analyzed by on-line gas chromatographs (GC). A GC with a packed molecular sieve 5A column (3 m, ∅1/4) and TCD were used to analyze H_2, N_2, CH_4, and CO. Another GC with a Gaskuropack 54 packed column (3 m, ∅1/4) and TCD were used to analyze CO_2, C_3H_6, and C_3H_8. The other hydrocarbons and the oxygenates were subjected to quantification by a GC with FID using a packed FFAP column (1 m, ∅1/4), but were not detected. All the lines and valves between the exit and the reactor and the gas chromatographs were heated to 120 °C to prevent condensation of the partial oxidation products.

3. Results and discussion

3.1. Structure and activity of Cr-MCM-41-DHT

Effects of metal species were tested by using Cr (57), Ga (46), Ni (46), V (40), Fe (51), Mn (47), and Co (45) on MCM-41 prepared by the DHT method (number in the parentheses shows Si/M ratios determined by ICP), among which Cr-MCM-41-DHT showed the highest activity, followed by Ga, Ni, V, Fe, Mn, and Co for the CO_2 dehydrogenation of C_3H_8 (Fig. 1). The data were corrected after the reaction for 0.5 h over each catalyst. Cr-MCM-41-DHT showed a yield above 15% with a high selectivity above 90% of propene. The order of the activities of these metals almost coincided with that observed over diamond-supported metal catalysts in the propane dehydrogenation [20]. When the Cr

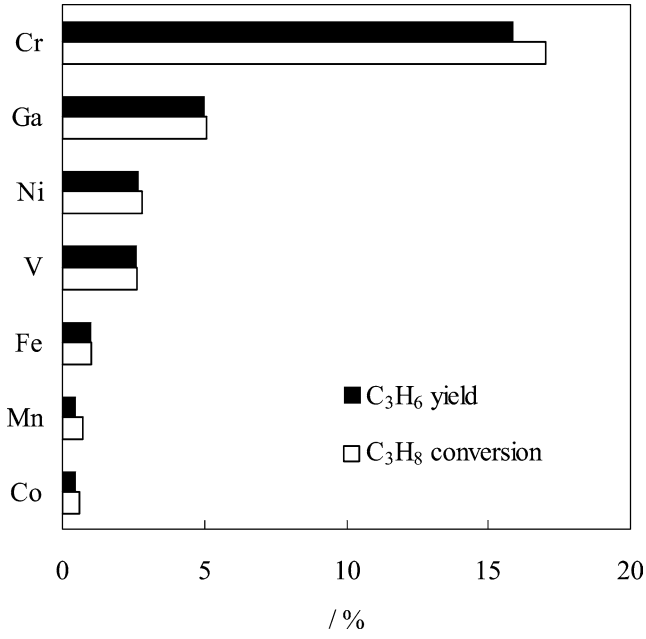

Fig. 1. The activity of various metals supported on MCM-41 with a Si/metal ratio of 50. Reaction conditions: catalyst weight, 400 mg; $P(C_3H_8)$ = 12.2 kPa; $P(CO_2)$ = 68.9 kPa; $P(N_2)$ = 20.3 kPa; reaction temperature, 550 °C; F = 0.134 mol(STP) h^{-1}.

Table 1
Properties of Cr-MCM-41 catalysts

Catalyst	Si/Cr[a]	Si/Cr[b]	Surface area ($m^2\ g_{cat}^{-1}$)	Pore volume ($cm^3\ g_{cat}^{-1}$)	Pore diameter (nm)
MCM-41	–	–	1025	0.94	2.7
Cr-MCM-41-DHT	100	165	878	0.79	2.7
Cr-MCM-41-DHT	75	91	829	0.72	2.7
Cr-MCM-41-DHT	50	57	780	0.70	2.7
Cr-MCM-41-DHT	25	23	629	0.36	2.7
Cr/Cab-O-Sil	50	55	163		
Cr/SiO_2	50	51	282		

[a] Calculated from the amount of raw materials.
[b] Determined by ICP analyses.

loading was changed on MCM-41-DHT, pore diameter was constant at 2.7 nm up to the Si/Cr ratio of 25, even though both pore volume and surface area decreased with increasing the Cr content (Table 1). Cr contents were determined by ICP analyses and are also shown in Table 1, indicating that all the metals in starting gel were not fully incorporated in silica structure. Both Cr/Cab-O-Sil and Cr/SiO_2 showed low values of surface area compared to Cr-MCM-41-DHT and no detectable pore volume. While MCM-41 was white, the color of Cr-MCM-41-DHT was pale green as synthesized and changed to pale yellow after the calcination at 550 °C for 6 h. XRD patterns at low diffraction angles showed four diffraction lines at $2\theta°$ of ca. 2.2, 3.6, 4.3, and 5.7° indexed to (100), (110), (200), and (210) of the regularity of hexagonal array of mesopores of MCM-41 for all the samples. The peak intensities for the Cr-MCM-41-DHT samples were not significantly lowered as compared with those for the purely silicious MCM-41, suggesting that the long-range regularity of hexagonal arrays of mesopores of MCM-41 was sustained after the introduction of chromium up to a content of 1.7 wt% (Si/Cr = 50). However, as Si/Cr ratio increased to 25 (3.4 wt% of the Cr content), these diffraction peaks significantly decreased, indicating a decrease in the structural regularity of the mesoporous structure at higher Cr content. This was clearly seen also in the drop in pore volume and surface area at a Si/Cr ratio of 25 (Table 1).

We have reported that only one kind of monochromate species was observed on Cr-MCM-41-DHT, whereas several types of chromate species possibly including both monochromates and polychromates existed on Cr-MCM-41-TIE by UV Raman spectroscopy [43]. Moreover, the two methods resulted in different locations of the accommodated metal cations: highly dispersed metal ions on the wall surface within MCM-41 mesopores for TIE, and monomeric metal species incorporated inside the framework of MCM-41 for DHT [42,43]. The chromium species in the as-synthesized samples by both methods exist in small Cr(III) oxide clusters with octahedrally coordinated chromium, and these species are transformed to chromate species with tetrahedrally coordinated Cr(VI) after the calcination.

Diffuse reflectance UV–vis spectra of Cr-MCM-41-DHT and Cr/Cab-O-Sil samples with both Si/Cr ratios of 50 are compared in Fig. 2. UV bands at 280 and 370 nm, which

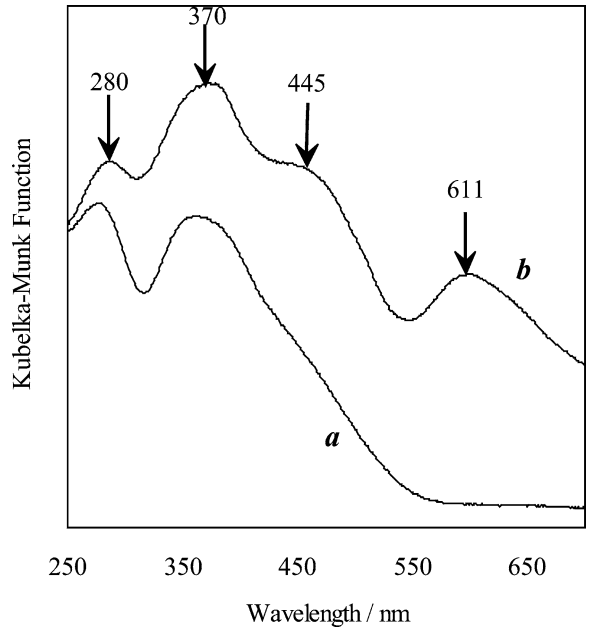

Fig. 2. Diffuse reflectance UV–vis spectra of Cr-MCM-41-DHT (a) and Cr/Cab-O-Sil (b) both with Si/Cr ratios of 50.

could be assigned to O–Cr(VI) charge transfer of chromates species [46], were mainly observed for both samples. A weak shoulder around 440 nm assigned to Cr(VI) polychromate was observed for Cr-MCM-41-DHT. The bands at 445 and 611 nm, characteristic for Cr/Cab-O-Sil, could be assigned to octahedral Cr(III) in Cr_2O_3 or CrO_x clusters, while the Cr(VI) species observed at 280 and 370 nm could be in tetrahedral coordination. Actually, the diffraction lines of Cr_2O_3 were clearly observed in XRD patterns of Cr/Cab-O-Sil, while no such line was observed with Cr-MCM-41-DHT and Cr/SiO_2, suggesting that Cr species are well dispersed on both Cr-MCM-41 and Cr/SiO_2 (Fig. 3). Differences in the dispersion of Cr species between Cr/Cab-O-Sil and Cr/SiO_2 may be partly due to the difference in surface area between Cab-O-Sil and SiO_2 (Table 1).

UV-Raman spectra of Cr-MCM-41-DHT and Cr/Cab-O-Sil samples both with Si/Cr ratios of 50 are shown in Fig. 4. We have reported that the use of a UV laser of 325 nm as the exciting source is a potent tool in distinguishing the

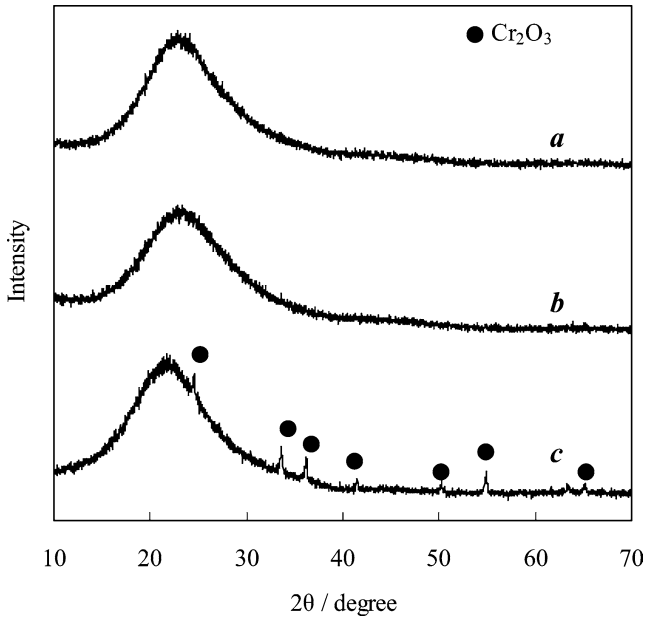

Fig. 3. XRD patterns of Cr-MCM-41-DHT (a), Cr/SiO_2 (b), and Cr/Cab-O-Sil (c) with Si/Cr ratios of 50.

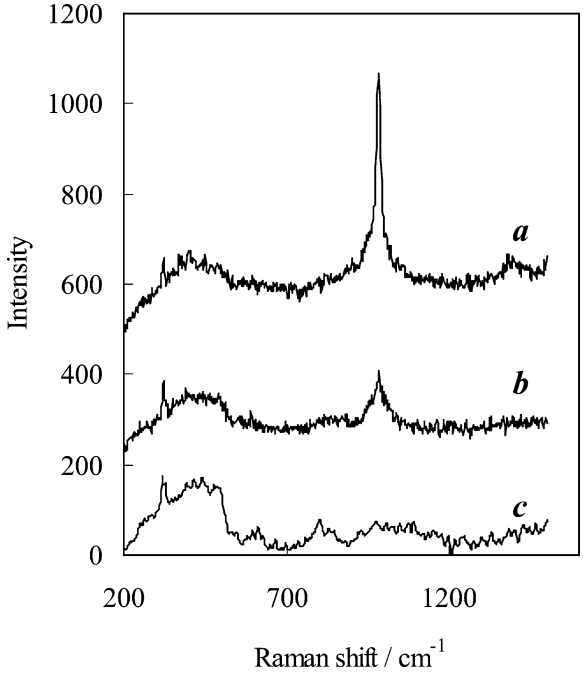

Fig. 4. UV-Raman spectra of Cr-MCM-41-DHT (a), Cr/Cab-O-Sil (b), and MCM-41 (c) with Si/Cr ratios of 50.

chromate species with different degrees of polymerization on MCM-41 [43]. In the present spectra, Cr-MCM-41-DHT showed an intense and sharp band at 980 nm assigned to the Cr–O stretching of dehydrated monochromate species (CrO_4^{2-}) [2]. This band was observed also with Cr/Cab-O-Sil though weakly. It is concluded that Cr-MCM-41-DHT possesses tetrahedrally coordinated $Cr(VI)O_4$, while Cr/Cab-O-Sil contains mainly polymeric chromates together with tetrahedrally coordinated $Cr(VI)O_4$ as a minor phase.

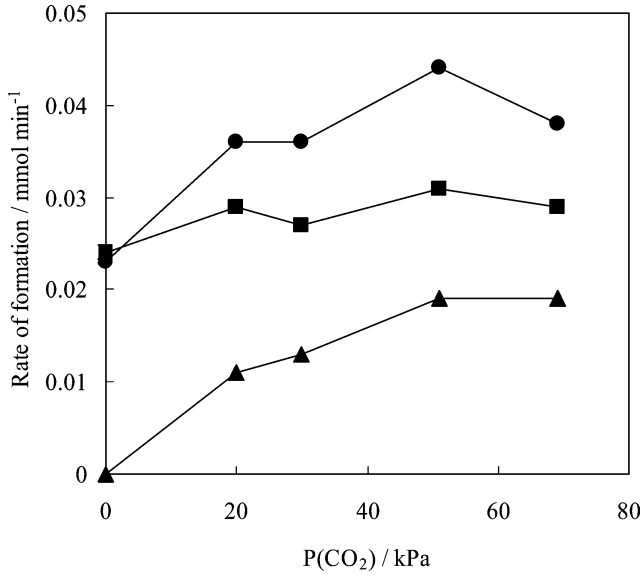

Fig. 5. CO_2 dehydrogenation of propane over Cr-MCM-41-DHT with a Si/Cr ratio of 50. Rate of formation: ●, C_3H_6; ■, H_2; ▲, CO. Reaction conditions: catalyst weight, 400 mg; $P(C_3H_8) = 12.2$ kPa; $P(CO_2) = 68.9$ kPa; $P(N_2) = 20.3$ kPa; reaction temperature, 550 °C; $F = 0.134$ mol(STP) h^{-1}.

3.2. Deactivation of the catalysts

As previously reported in the results of CO_2 dehydrogenation of propane over Cr-MCM-41 DHT with various Cr contents at 550 °C [43], the selectivity to C_3H_6 was always higher than 90% and the conversion of C_3H_8 increased almost linearly with an increase in the Cr content. Even though the BET surface area and pore volume decreased largely as the Cr content increased to 3.4 wt% (Si/Cr = 25) (Table 1), the conversion of C_3H_8 and the yield of C_3H_6 still increased with the Cr content, indicating that changes in the porous structure did not significantly influence the catalytic behavior. The rates of formations of C_3H_6, H_2, and CO are shown in Fig. 5. All data were corrected at the reaction time of 0.5 h. Even in the absence of CO_2, C_3H_8 was dehydrogenated to C_3H_6 accompanied by H_2 formation, suggesting that simple dehydrogenation of C_3H_8 took place over Cr-MCM-41-DHT. The rate of C_3H_6 formation remarkably increased together with that of CO formation with increasing the partial pressure of CO_2. On the other hand, the rate of H_2 formation showed no significant increase even with increasing the partial pressure of CO_2. In all reactions, the selectivity to C_3H_6 was always around 95% and small amounts of C_2H_6, C_2H_4, and CH_4 were formed. According to the thermodynamic equilibrium of the dehydrogenation of propane

$$CH_3CH_2CH_3 = CH_2{=}CHCH_3 + H_2, \quad (1)$$

at 550 °C in the gas mixture of N_2–He–C_3H_8 at a molar ratio of 10:34:6 and at $F = 0.134$ mol(STP) h^{-1}, propane conversion is calculated as 60.8%. As shown by thermodynamic considerations [16], propane conversion can be improved by

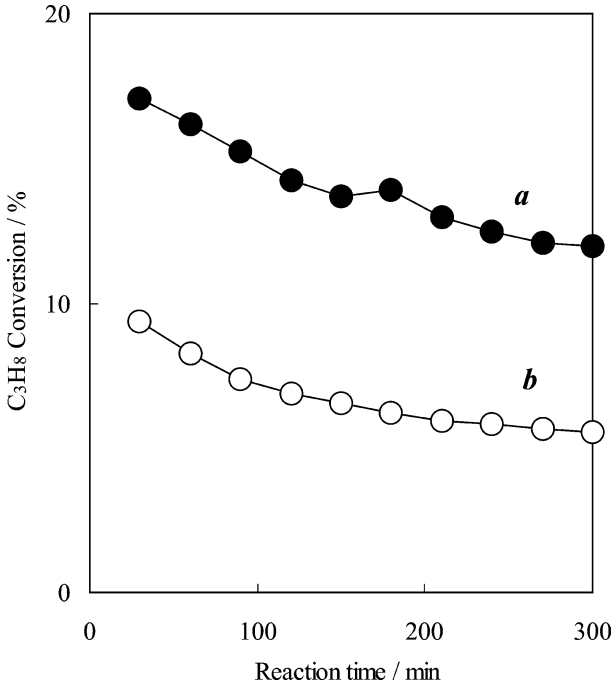

Fig. 6. Deactivation of Cr-MCM-41-DHT catalysts during the reaction. Reaction conditions: catalyst weight, 400 mg; reaction temperature, 550 °C; $F = 0.134$ mol(STP) h^{-1}; (a) $P(C_3H_8) = 12.2$ kPa; $P(CO_2) = 68.9$ kPa; $P(N_2) = 20.3$ kPa; (b) $P(C_3H_8) = 12.2$ kPa; $P(He) = 68.9$ kPa; $P(N_2) = 20.3$ kPa.

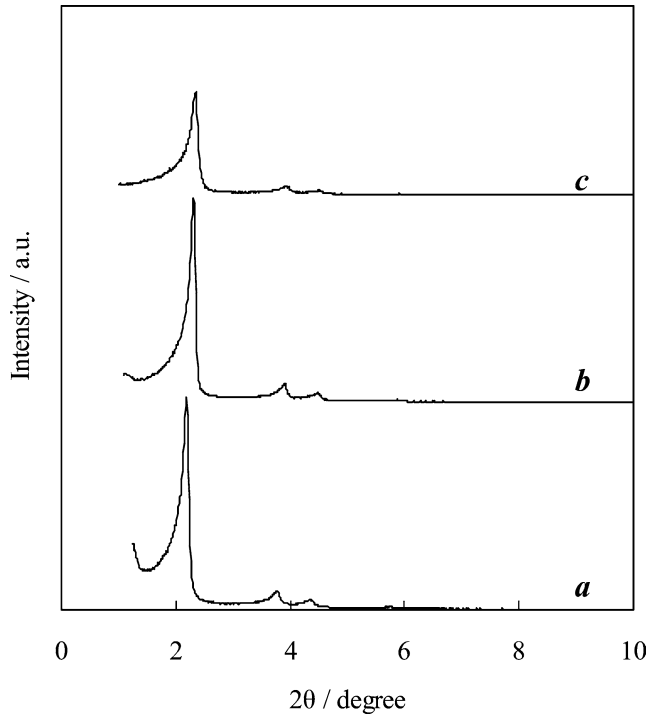

Fig. 7. XRD patterns of Cr-MCM-41-DHT with Si/Cr ratios of 50. (a) Before the reaction, (b) after the reaction under CO_2 atmosphere, and (c) after the reaction under He atmosphere.

coupling the reaction with the water–gas-shift reaction

$$H_2 + CO_2 = CO + H_2O. \quad (2)$$

As the result, the dehydrogenation equilibrium is shifted toward products under a CO_2 atmosphere. The value obtained in the present work was below 30% and far lower than the value of 60.8% when the reaction proceeds by simple dehydrogenation (1). This suggests that the catalyst was not active enough, quickly deactivated during the reaction, or the regeneration was too slow to keep the catalyst in the active form (vide infra).

Cr-MCM-41-DHT (Si/Cr = 50) showed a C_3H_8 conversion of 17.0% with a C_3H_6 yield of 15.9% with a gas mixture of N_2–CO_2–C_3H_8 at a molar ratio of 10:34:6 and at $F = 0.134$ mol(STP) h^{-1} (Fig. 6). The activity gradually decreased during the reaction over the Cr-MCM-41-DHT, indicating catalyst deactivation (Fig. 6, a). A similar deactivation was also observed under a He atmosphere in the absence of CO_2 (Fig. 6, b). In the XRD patterns for the Cr-MCM-41-DHT after the reactions, the peak intensities at the low diffraction angles significantly decreased under a He atmosphere (Fig. 7, c) as compared with those for that under a CO_2 atmosphere (Fig. 7, b), suggesting that the long-range regularity of hexagonal arrays of mesopores of MCM-41 was weakened after the reaction in He. Also both surface area and pore volume were significantly decreased under a He atmosphere, but not substantially affected under a CO_2 atmosphere (Table 2). This suggests that lattice oxygen in Cr-MCM-41-DHT was consumed during the dehydrogenation under He atmosphere, resulting in the corruption or the weakening of the long-range regularity of hexagonal arrays, while the defect formed by the lattice oxygen uptake can be refilled by oxygen from gas-phase CO_2, resulting in no substantial change in the structure under a CO_2 atmosphere.

Table 2
Properties of Cr-MCM-41-DHT (Si/Cr = 50) catalysts[a] after the reaction

Reaction atmosphere	Surface area ($m^2\ g_{cat}^{-1}$)	Pore volume ($cm^3\ g_{cat}^{-1}$)	Pore diameter (nm)
–[b]	781	0.61	2.7
CO_2[c]	782	0.61	2.7
He[d]	719	0.47	2.7

[a] Catalysts were pressed at 4.2 MPa, crushed and meshed to particle sizes of 0.3–0.5 mm.
[b] Before the reaction.
[c] After the reaction for 5 h with $N_2/CO_2/C_3H_8 = 10/34/6$ (ml min^{-1}).
[d] After the reaction for 5 h with $N_2/He/C_3H_8 = 10/34/6$ (ml min^{-1}).

According to the Cr-K-edge XANES spectra for the Cr-MCM-41-DHT sample with a Si/Cr ratio of 50 (Fig. 8A, a–d), a preedge peak was clearly observed before the reaction, while this peak was significantly weakened even after the reaction for 0.5 h and the edge position shifted to lower energy during the reaction, suggesting that the local symmetry around the chromium center has been changed from tetrahedral coordination to octahedral coordination during the reaction [43,47]. In the results of Fourier transforms of k^3-weighted Cr-K-edge EXAFS (Fig. 8B, a), a single peak was observed before the reaction and could be assigned to the bond of Cr–O, consisting of two Cr=O bonds and two

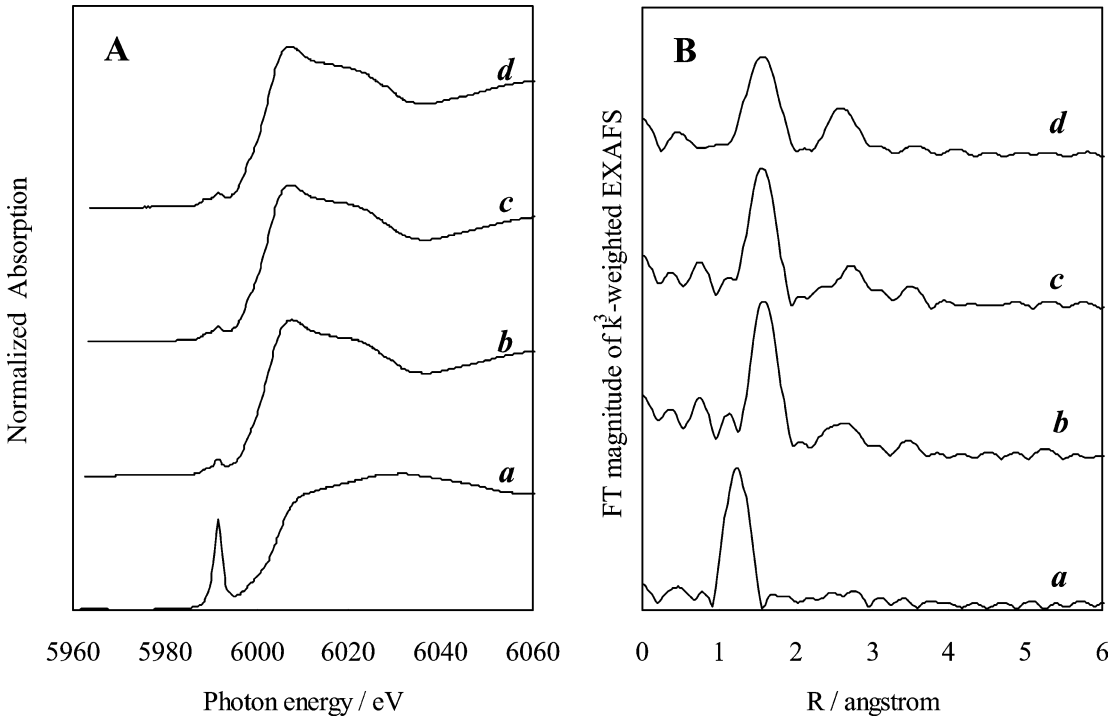

Fig. 8. Cr-K-edge XANES spectra (A) and Fourier transforms of k^3-weighted Cr-K-edge EXAFS (B) for the Cr-MCM-41-DHT sample with a Si/Cr ratio of 50 during the reaction under CO_2 atmosphere. (a) Before the reaction, (b) after the reaction for 0.5 h, (c) after the reaction for 1 h, and (d) after the reaction for 5 h.

Cr–O bonds in CrO_4 tetrahedra (vide infra). After the reaction for 0.5 h (Fig. 8B, b), two distinct peaks appeared at 1.6 and 2.6 Å (non-phase-shift corrected) and the intensity of the latter peak increased, while that of the first one decreased, during the reaction (Fig. 8B, c and d). Similarly two peaks were also observed for Cr_2O_3 or Cr/Cab-O-Sil and could be assigned to the bonds of Cr–O in CrO_6 octahedra and Cr–O–Cr through corner-shared CrO_6 octahedra [48]. The increase in the intensity of the latter peak indicates that aggregation of Cr species took place during the reaction. However, the peak in the vicinity of 3.3 Å (non-phase-shift corrected) was relatively weak as compared with that for Cr_2O_3. Thus, it is reasonable to consider that the chromium species exist as small $Cr(III)O_x$ clusters after the dehydrogenation reaction, although it is difficult to determine the size of the clusters [49].

The results obtained by curve fitting of Fourier transforms of k^3-weighted Cr-K-edge EXAFS are shown in Table 3, which confirm the tetrahedral coordination of chromium (total coordination number = 3.9) for the sample before the reaction. However, the four Cr–O bonds of the CrO_4 tetrahedron are not equivalent; two of the Cr=O bonds are shorter (1.66 Å) and the other two are relatively longer (1.85 and 2.01 Å, respectively). The two shorter Cr–O bonds may possess a double-bond nature and the other two possess a single-bond nature. After the reaction for 0.5 h under a CO_2 atmosphere, the structure was totally changed to the octahedral coordination (total coordination number = 6.1). In this case, too, the six Cr–O bonds of the CrO_6 octahedron are not equivalent, three of the Cr–O bonds are shorter (1.97 Å), and the other three are relatively longer (2.06 Å). Considering the results of both diffuse reflectance UV–vis spectra (Fig. 2) and X-ray absorption spectra (Fig. 8 and Table 2), it is concluded that tetrahedrally coordinated $Cr(VI)O_4$ exists on Cr-MCM-41-DHT before the reaction and reduced to octahedrally coordinated $Cr(III)O_6$ during the reaction. It is also noteworthy that the latter species appeared as polychromates on Cr-MCM-41-DHT, the sizes of which are too small to be observed in XRD, while chromium species on Cr/Cab-O-Sil always appeared as Cr_2O_3 detectable by XRD.

Table 3
Parameters obtained from EXAFS analysis for the Cr-MCM-41 catalysts before the reaction and after the reaction

Sample	Shell	CN[a]	R (Å)[b]	$\Delta\sigma^2$ (Å^2)[c]
Before the reaction	Cr–O	2.0	1.66	−0.0047
		0.9	1.85	−0.0057
		1.0	2.01	0.0064
After the reaction[d]	Cr–O	3.0	1.97	−0.0005
		3.1	2.06	0.0016

[a] Coordination number.
[b] Bond length (Å).
[c] Debye–Waller factor (Å^2).
[d] The data were corrected after the reaction for 0.5 h under CO_2.

3.3. Regeneration of the catalysts with O_2

During the reaction over Cr-MCM-41-DHT and Cr/Cab-O-Sil catalysts both with Si/Cr ratios of 50, the conversion

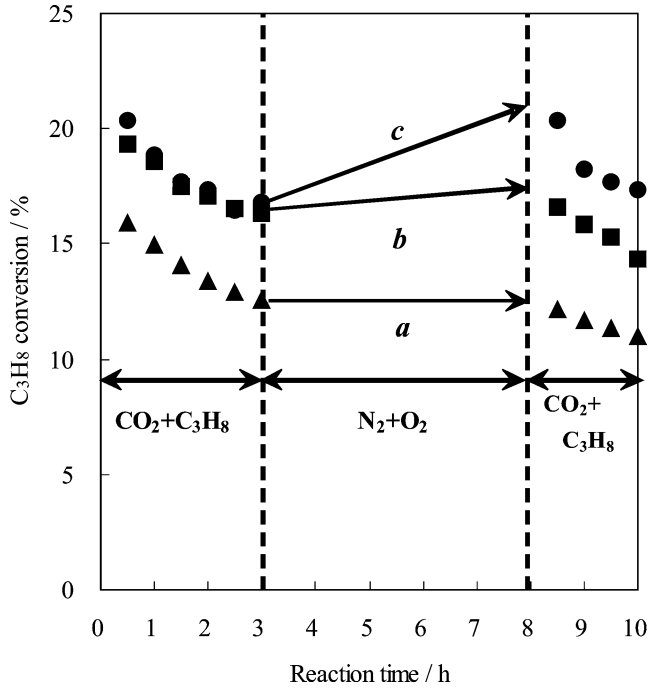

Fig. 9. Effect of O_2 treatment of deactivated catalysts. Cr/Cab-O-Sil (Si/Cr = 50), (b) Cr/SiO_2 (Si/Cr = 50), (c) Cr-MCM-41-DHT (Si/Cr = 50). Reaction conditions: catalyst weight, 400 mg; $P(C_3H_8) = 12.2$ kPa; $P(CO_2) = 68.9$ kPa; $P(N_2) = 20.3$ kPa; $P(O_2) = 12.2$ kPa; reaction temperature, 550 °C.

of C_3H_8 gradually decreased, indicating a deactivation of the catalyst also on Cr/Cab-O-Sil (Fig. 9). After the reaction for 3 h, the gas flow of the mixture of C_3H_8 and CO_2 was stopped and replaced by the mixed gas flow of O_2 and N_2 at a ratio of 10/10 ml min^{-1}. After the treatment with O_2 for 5 h, the reaction was again started by replacing the gas flow with a mixture of C_3H_8 and CO_2. The activity of Cr-MCM-41 was recovered as seen by the fact that C_3H_8 conversion returned to the original value (Fig. 9, c), but that of Cr/Cab-O-Sil was not recovered at all (Fig. 9, c), after the treatment with O_2. Cr/SiO_2 showed an insufficient but detectable recovery of the activity after the O_2 treatment (Fig. 9, b). When these three catalysts were again put under the reaction conditions after the O_2 treatment, the conversion of C_3H_8 decreased in an almost similar way to the first reaction step in every case.

The results of X-ray absorption spectroscopic measurements for Cr-MCM-41-DHT during the O_2 treatment are shown in Fig. 10. As previously noted, the changes in both XANES (Fig. 10A, a and b) and the EXAFS (Fig. 10B, a and b) spectra indicate that the $Cr(VI)O_4$ tetrahedra were reduced to an aggregated form of the $Cr(III)O_6$ octahedra during the reaction for 3 h. After the treatment with O_2, the XANES (Fig. 10A, c) and the EXAFS spectra (Fig. 10B, c) showed a sharp preedge peak and a single peak, respectively, suggesting that the $Cr(VI)O_4$ tetrahedra were regenerated by the reoxidation of the $Cr(III)O_6$ octahedra. Moreover, the $Cr(VI)O_4$ tetrahedra were again changed to the $Cr(III)O_6$ octahedra after the second reaction for 0.5 h (Figs. 10A and 10B, d). The curve-fitting results for the Cr–O shell confirmed that the coordination structure of chromium was changed from tetrahedral to octahedral even after 1 h of the reaction of C_3H_8 dehydrogenation. These changes in the coordination structure correlated well with the phenomena of

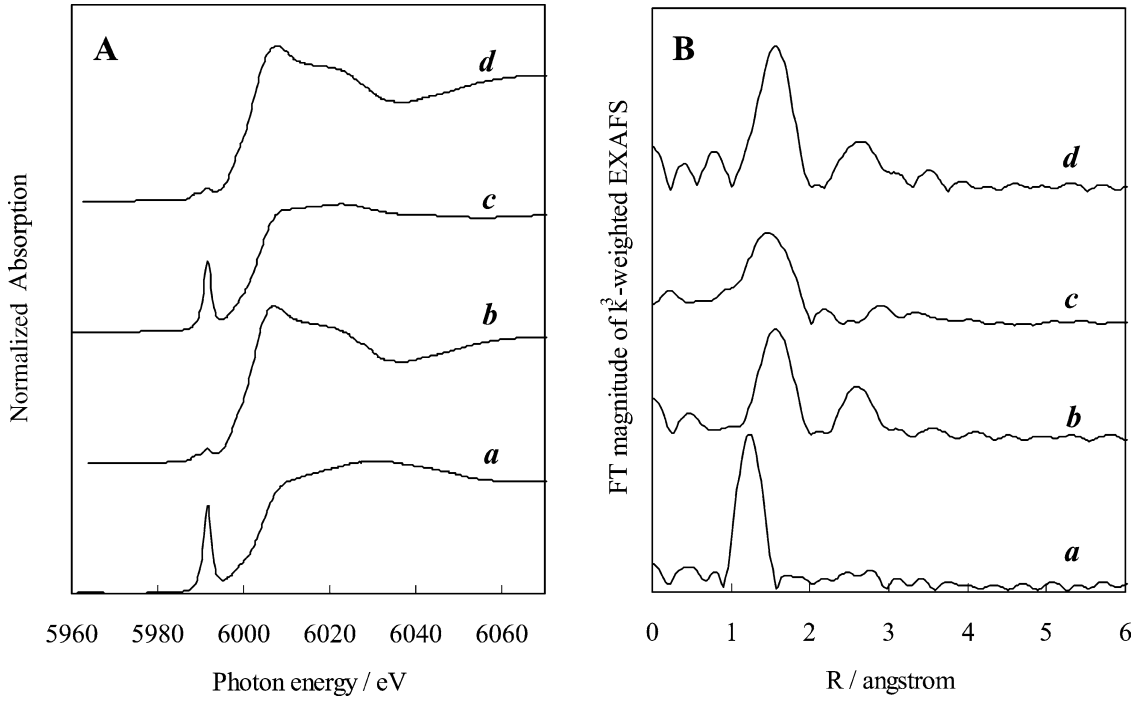

Fig. 10. Cr-K-edge XANES spectra (A) and Fourier transforms of k^3-weighted Cr-K-edge EXAFS (B) for the Cr-MCM-41-DHT sample with a Si/Cr ratio of 50. (a) Before the first reaction, (b) after the first reaction for 3 h, (c) after treatment with O_2, and (d) after the second reaction for 0.5 h.

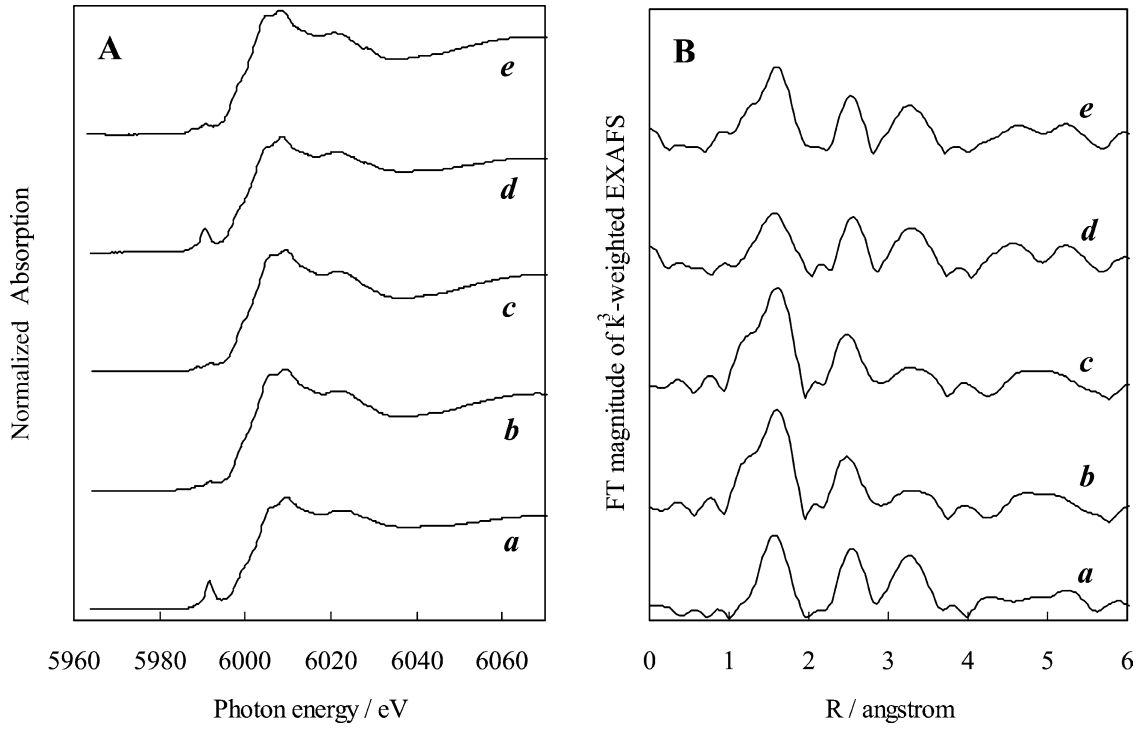

Fig. 11. Cr-K-edge XANES spectra (A) and Fourier transforms of k^3-weighted Cr-K-edge EXAFS (B) for the Cr/Cab-O-Sil sample with the Si/Cr ratio of 50. (a) Before the reaction, (b) after the reaction for 0.5 h, (c) after the reaction for 1 h, (d) after the treatment with O_2, and (e) after the second reaction for 1 h.

deactivation and activity regeneration shown in Fig. 9, c. It is suggested that the terahedrally coordinated Cr(VI) plays an important role in the dehydrogenation of C_3H_8 with CO_2. XRD measurements showed no diffraction line assigned to any chromium species during all processes, i.e., the dehydrogenation reaction, the O_2 treatment, and the second dehydrogenation reaction, suggesting that the particle size of the aggregated form of the Cr(III)O_6 octahedra was too small to be detected by XRD.

On the other hand, in the XANES and EXAFS spectra for the Cr/Cab-O-Sil (Fig. 11), the preedge peak was weak even before the reaction (Fig. 11A, a) and two peaks assigned to each bond of Cr–O in Cr(III)O_6 octahedra and Cr–O–Cr through corner-shared Cr(III)O_6 octahedra were always observed both before and after the reaction (Fig. 11B, a, b, and c). Even after the treatment with O_2 (Fig. 11, d), no significant change was observed in both XANES and EXAFS spectra except that the preedge peak was weakly enhanced. These results are almost well coincident with the phenomena of activity change of Cr/Cab-O-Sil during the treatment with O_2 (Fig. 9, b); i.e., no significant recovery in the activity was observed even after the treatment with O_2. According to the results of curve deconvolution of the EXAFS spectrum of Cr/Cab-O-Sil, it is estimated that the spectrum consisted of 30% tetrahedral and 70% octahedral coordination. No significant change was observed in this spectrum during the reaction, even before and after the treatment with O_2. A diameter of Cr_2O_3 particles on Cr/Cab-O-Sil calculated by the Scherrer equation from the results of XRD was 35–40 nm during all processes, i.e., the dehydrogenation reaction, the O_2 treatment, and the second dehydrogenation reaction, suggesting that the particle size of Cr_2O_3 was not significantly affected by the reaction atmosphere.

3.4. Regeneration of active site with CO_2

The results of temperature-programmed reduction measurements for Cr-MCM-41-DHT and Cr/Cab-O-Sil catalysts with both Si/Cr ratios of 50 are shown in Fig. 12. In the first TPR of Cr-MCM-41-DHT (Fig. 12A, a), an intense peak was observed between 350 and 600 °C and is probably attributed to the reduction of Cr(VI) or Cr(V) to Cr(III) [50]. After the first TPR, the sample was cooled to ambient temperature, followed by the second TPR under the same conditions. The intense peak observed between 350 and 600 °C in the first TPR disappeared in the second TPR (Fig. 12A, b), suggesting that all reducible chromium species were reduced in the first TPR. Then, the sample was again cooled and treated with CO_2 gas flow at a rate of 20 ml min^{-1} at 550 °C for 1 h. After the treatment with CO_2, the third TPR was carried out under the same conditions as above. The reduction peak was again observed between 350 and 600 °C in the third TPR (Fig. 12A, c) and the peak area was 71% of that observed in the first TPR (Fig. 12A, a).

A similar peak change was observed also in the TPR of Cr/Cab-O-Sil (Fig. 12B), even though the reduction peak area was far smaller than that of Cr-MCM-41. In the first TPR (Fig. 12B, a), the reduction peak was observed between 350 and 600 °C and the peak area was less than half of that observed on Cr-MCM-41-DHT, suggesting that the

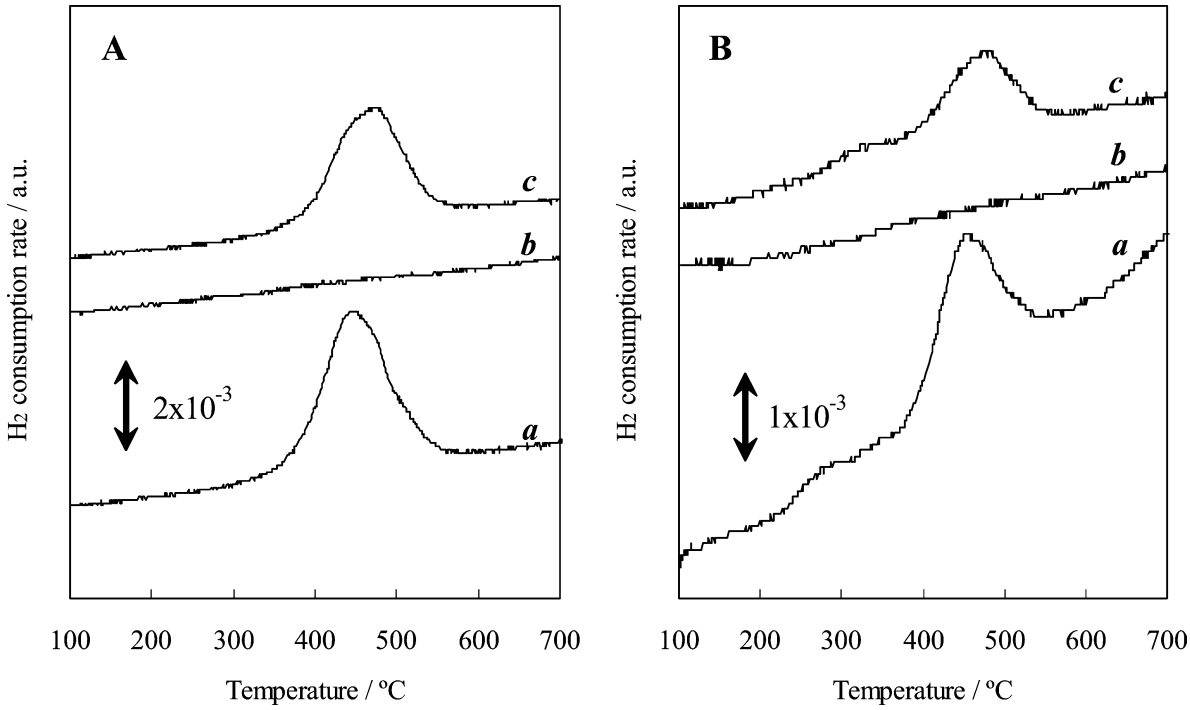

Fig. 12. Temperature-programmed reduction of Cr-MCM-41-DHT (A) and Cr/Cab-O-Sil (B) sample both with Si/Cr ratios of 50. (a) The first TPR, (b) the second TPR, (c) the third TPR after the treatment with CO_2.

amount of Cr(VI) or Cr(V) on Cr/Cab-O-Sil was far smaller than that on Cr-MCM-41-DHT. No reduction peak was observed in the second TPR (Fig. 12B, b), and the reduction peak appeared in the third TPR after the treatment with CO_2 (Fig. 12B, c). The peak area in the third TPR was 50% of that observed in the first TPR, suggesting that reoxidation of Cr(III) formed on Cr/Cab-O-Sil is more difficult than that on Cr-MCM-41-DHT.

The results of X-ray absorption spectroscopic measurements for the Cr-MCM-41-DHT sample during the treatment with H_2 and then with CO_2 are shown in Fig. 13. Both XANES and EXAFS spectra of the sample before the first TPR are shown in Fig. 13A, a, and Fig. 13B, a, respectively. The sample was first treated under a mixture of 5 vol% H_2/Ar at a flow rate of 100 ml min^{-1} by increasing the temperature from ambient temperature to 600 °C. After the H_2 treatment, a preedge peak was significantly weakened in the XANES spectra (Fig. 13A, b) and a single peak was shifted to double peaks in the EXAFS spectra (Fig. 13B, b). As previously noted, the changes in both XANES and EXAFS spectra indicate that the $Cr(VI)O_4$ tetrahedra was reduced to the aggregated form of the $Cr(III)O_6$ octahedra during the H_2 treatment. Then, the sample was treated with CO_2 at a flow rate of 20 ml min^{-1} at 550 °C for 1 h. After the treatment with CO_2, both XANES (Fig. 13A, c) and EXAFS (Fig. 13B, c) spectra recovered their original forms; i.e., the former and the latter showed a sharp preedge peak and an almost single peak, respectively, suggesting that the $Cr(VI)O_4$ tetrahedra were regenerated by the reoxidation of the $Cr(III)O_6$ octahedra with CO_2.

3.5. Coke formation on the catalysts

The coke amount estimated by TPO measurement of the catalyst after the dehydrogenation reaction of C_3H_8 with CO_2 for 5 h is shown in Table 4. On each 0.4 g of Cr-MCM-41-DHT, Cr/SiO_2, and Cr/Cab-O-Sil catalysts, 0.73, 1.52, and 0.50 mg of coke were formed after the reaction, respectively. Larger amounts of coke deposited on all catalysts under a CO_2 atmosphere than under a He atmosphere. Coke can be formed more intensively on the catalyst surface from C_3H_6 than from C_3H_8, and therefore the enhanced formation of C_3H_6 generally resulted in a larger amount of coke formation except for the largest amount of coke over Cr/SiO_2. It was clearly observed that CO was produced from CO_2 during the C_3H_8 dehydrogenation over Cr-MCM-41-DHT with the Si/Cr ratio of 50 (Fig. 5). It was noted that CO_2 can work as an oxidizing agent of the reduced octahedral $Cr(III)O_6$ species to the tetrahedral $Cr(VI)O_4$ species as observed in the results of TPR (Fig. 12) and X-ray absorption spectroscopy (Fig. 13). Moreover it must be noted that CO_2 can be converted to CO via a reverse water–gas-shift reaction by consuming H_2 or via a Boudouard reaction by consuming coke on the catalyst surface.

Nakagawa et al. [51,52] reported that CO_2 suppressed coke formation on the catalyst in the dehydrogenation of ethane with CO_2 over Ga_2O_3/TiO_2, while Sakurai et al. [53,54] reported that, in the dehydrogenation of ethylbenzene with CO_2 over V_2O_5/MgO, coke formation on the catalyst was rather enhanced in an atmosphere of CO_2 than Ar. Furthermore, it was considered that the acidic site of the

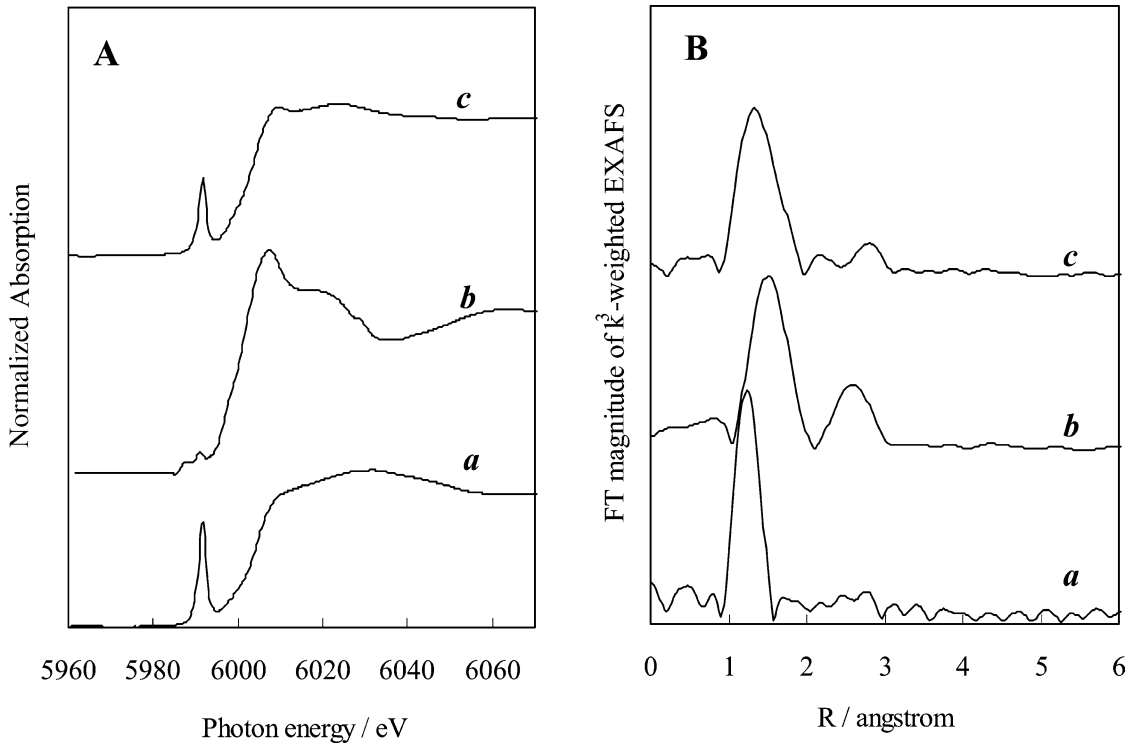

Fig. 13. Cr-K-edge XANES spectra (A) and Fourier transforms of k^3-weighted Cr-K-edge EXAFS (B) for the Cr-MCM-41-DHT sample with a Si/Cr ratio of 50. (a) Before the first TPR, (b) after the first TPR, and (c) after treatment with CO_2.

Table 4
Coke amount after the reaction[a]

Catalyst	Reaction atmosphere	Coke amount (mg g_{cat}^{-1})
Cr-MCM-41-DHT	CO_2[b]	1.83
	He[c]	0.60
Cr/Cab-O-Sil	CO_2[b]	1.25
	He[c]	0.53
Cr/SiO_2	CO_2[b]	3.80
	He[c]	2.33

[a] Catalysts were pressed at 4.2 MPa, crushed and meshed to particle sizes of 0.3–0.5 mm, and 0.2 g was used in the reaction for 5 h.
[b] $N_2/CO_2/C_3H_8 = 10/34/6$ (ml min^{-1}).
[c] $N_2/He/C_3H_8 = 10/34/6$ (ml min^{-1}).

Ga_2O_3/TiO_2 catalyst would be the active site of the dehydrogenation of ethane, and CO_2 might promote rapid desorption of product from the surface of the catalyst, resulting in a lowering of coke formation [52]. On the other hand, V_2O_5/MgO seems to catalyze the dehydrogenation of ethylbenzene with CO_2 via its reduction–oxidation mechanism; i.e., CO_2 behaves as an oxidant for the vanadium species, and the surface vanadium species are kept in a high oxidation state with CO_2 during the reaction. Active phases of vanadium in the dehydrogenation reaction were believed to be V(V) species in V_2O_5 or $Mg_3V_2O_8$ on highly dispersed MgO [54].

Also on the present Cr-MCM-41-DHT catalyst, it is considered that the reaction proceeds via the reduction–oxidation of Cr species. During the dehydrogenation with CO_2, tetrahedrally coordinated $Cr(VI)O_4$ species are reduced to an aggregated form of octahedrally coordinated $Cr(III)O_6$ species and the latter species can be reoxidized by CO_2 (Figs. 12 and 13). The behavior of the Cr-MCM-41-DHT catalyst is similar to that of V_2O_5/MgO, and CO_2 could not suppress the coke formation on both catalysts. It is likely that coke formed from propene as a main product and its high concentration possibly resulted in a large amount of coke formation. However, as seen in Fig. 9, no regeneration of the activity was observed on both Cr/SiO_2 and Cr/Cab-O-Sil, even though coke on both catalysts was almost eliminated during the oxidation treatment for 5 h. On the other hand, the activity was quickly regenerated on Cr-MCM-41-DHT even after the oxidation treatment for a short time, i.e., 1 h, during which coke elimination was not completed. Both completed and noncompleted coke elimination was confirmed by GC analyses during the oxidation treatment.

Effects of pretreatments of Cr-MCM-41-DHT (Si/Cr = 50) under O_2 or H_2 atmospheres are shown in Fig. 14. H_2 treatment was carried out under the TPR conditions, i.e., with H_2/Ar (5/95 ml min^{-1}) from room temperature to 700 °C at a rate of 10 °C min^{-1} as shown in Fig. 12, expecting that Cr(VI) or Cr(V) was completely reduced to Cr(III). Oxidation treatment with O_2/N_2 (10/10 ml min^{-1}) at 550 °C for 1 h was effective for keeping the catalyst in the active form as seen in the highest propane conversion obtained in dehydrogenation with CO_2 (a), followed by the reaction under He atmosphere (b), among the reactions tested. On the other hand, the reduction treatment with H_2 resulted in a substantial decrease in the activity. On the reduced catalyst,

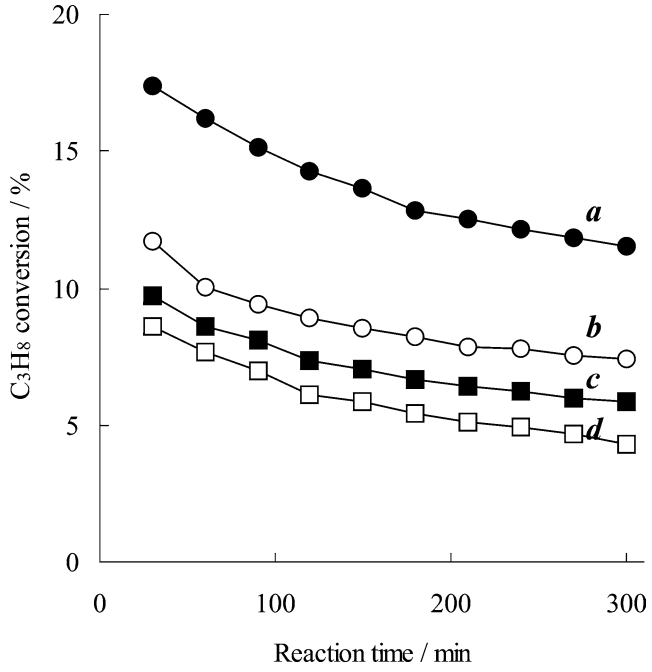

Fig. 14. Effect of pretreatment of Cr-MCM-41-DHT catalyst with the Si/Cr ratio of 50. Cr-MCM-41-DHT was pretreated under the following conditions: (a and b) with O_2/N_2 (10/10 ml min^{-1}) at 550 °C for 1 h, followed by the reaction under CO_2 (a) or He (b); (c and d) with H_2/Ar (5/95 ml min^{-1}) from room temperature to 700 °C at a rate of 10 °C min^{-1}, followed by the reaction under CO_2 (c) or He (d). Reaction conditions: catalyst weight, 400 mg; $P(C_3H_8) = 12.2$ kPa; $P(CO_2) = 68.9$ kPa; $P(He) = 68.9$ kPa; $P(N_2) = 20.3$ kPa; reaction temperature, 550 °C.

propane conversion was low even with CO_2 (c) and further decreased under a He atmosphere (d). As a result, it is concluded that the reduction treatment showed a definitive role in the deactivation of Cr-MCM-41 catalysts. The reoxidizing ability of CO_2 is not high enough to keep Cr species in the state of Cr(VI)O_4 and therefore the activity decreased during the reaction. Finally, the activity was recovered by the treatment with O_2, again resulting in the reoxidation of Cr(III)O_6 to Cr(VI)O_4 (Fig. 9). The deactivation of catalyst is frequently attributed to coke formation on the catalyst surface. Also in the present reaction, coke can be removed by the treatment with O_2 or by the Boudouard reaction with CO_2, possibly resulting in the recovery of the activity. However, even though coke is eliminated and the catalyst can be reactivated during the reoxidation treatment with O_2 or with CO_2, the contribution of the regeneration of Cr(VI)O_4 tetrahedra is more strongly suggested as the mechanism of activity recovery of Cr-MCM-41-DHT.

4. Conclusion

Cr-MCM-41 catalysts prepared by direct hydrothermal synthesis showed high activity in the dehydrogenation of propane with carbon dioxide, resulting in the production of propene with a conversion of 30% and a selectivity above 90%. It is suggested that Cr(VI) in tetrahedral coordination formed as an active monochromate species and reduced to Cr(III) in octahedral coordination as a less active polychromate species during the reaction. Deactivated catalyst was regenerated by a treatment with gaseous oxygen, during which the reoxidation of the Cr(III) species to the Cr(VI) species was observed. Not only gaseous oxygen but also carbon dioxide could regenerate Cr(VI)O_4 tetrahedra from reduced Cr(III)O_6 octahedra, even though the efficiency of carbon dioxide was lower than that of oxygen. It is concluded that during the reaction propane is dehydrogenated to propene by Cr(IV)O_4 tetrahedra, which is simultaneously reduced to Cr(III)O_6 octahedra. The reduced Cr(III)O_6 octahedra can be reoxidized to Cr(VI)O_4 tetrahedra by carbon dioxide, and thus the reduction–oxidation cycle between Cr(VI)O_4 tetrahedra and Cr(III)O_6 octahedra has an important role in the dehydrogenation of propane with carbon dioxide over Cr-MCM-41.

Acknowledgment

The X-ray absorption measurements were performed under the approval of the Photon Factory (KEK-PF) Program Advisory Commitee (Proposal No. 2002G097).

References

[1] J. Muzart, Chem. Rev. 92 (1992) 113.
[2] B.M. Weckhuysen, I.E. Wachs, R.A. Schoonheydt, Chem. Rev. 96 (1996) 3327.
[3] L.R. Mentasty, O.F. Gorriz, L.E. Cadus, Ind. Eng. Chem. Res. 38 (1999) 389.
[4] A. Hakuli, M.E. Harlin, L.B. Backman, A.O.I. Krause, J. Catal. 184 (1999) 349.
[5] B. Crzybowska, J. Słoczyński, R. Grabowski, K. Wcisło, A. Kozłowska, J. Stoch, J. Zieliński, J. Catal. 178 (1998) 687.
[6] A. Jimenez-Lopez, E. Rodriguez-Castellon, P. Maireles-Torres, L. Diaz, J. Merida-Robles, Appl. Catal. A 218 (2001) 295.
[7] S.M. Al-Zahrani, N.O. Elbhasir, A.E. Abasaeed, M. Abdulwashed, Ind. Eng. Chem. Res. 40 (2001) 781.
[8] M. Cherian, M.S. Rao, A.M. Hirt, I.E. Wachs, G. Deo, J. Catal. 211 (2002) 482.
[9] M. Hoang, J.F. Mathews, K.C. Pratt, J. Catal. 171 (1997) 320.
[10] J. El-Idrissi, M. Kacimi, F. Bozon-Verduraz, M. Ziyad, Catal. Lett. 56 (1998) 221.
[11] S. de Rossi, M.P. Casaletto, G. Ferrais, A. Cimino, G. Minelli, Appl. Catal. A 167 (1998) 257.
[12] C.M. Pradier, F. Rodriguez, P. Marcus, M.V. Landau, M.L. Laliya, A. Gutman, M. Herskowitz, Appl. Catal. B 27 (2000) 73.
[13] M.L. Parentis, N.A. Bonini, E.E. Gonzo, React. Kinet. Catal. Lett. 76 (2002) 243.
[14] A.I. Tsyganok, T. Tsunoda, S. Hamakawa, K. Suzuki, K. Takehira, T. Hayakawa, J. Catal. 213 (2003) 191.
[15] T. Nishiyama, K. Aika, J. Catal. 122 (1990) 346.
[16] S. Wang, K. Murata, T. Hayakawa, S. Hamakawa, K. Suzuki, Appl. Catal. A 196 (2000) 1.
[17] X. Ge, M.M. Zhu, J.Y. Shen, React. Kinet. Catal. Lett. 77 (2002) 103.
[18] N. Mimura, I. Takahara, M. Inaba, M. Okamoto, K. Murata, Catal. Commun. 3 (2002) 257.
[19] I. Takahara, W.C. Chang, N. Nimura, M. Saito, Catal. Today 45 (1998) 55.

[20] K. Nakagawa, C. Kajita, N. Ikenaga, M. Nishitani-Gamo, T. Ando, T. Suzuki, Catal. Today 84 (2003) 149.
[21] S.M. Al-Zahrani, B.Y. Jibril, A.E. Abasaeed, Catal. Today 81 (2003) 507.
[22] M. Cherian, M.S. Rao, G. Deo, Catal. Today 78 (2003) 397.
[23] K.L. Fujdala, T.D. Tilley, J. Catal. 218 (2003) 123.
[24] M. Cherian, M.S. Rao, W.-T. Yang, J.-M. Jehng, A.M. Hirt, G. Deo, Appl. Catal. A 233 (2002) 21.
[25] P. Moriceau, B. Grzybowska, L. Gengembre, Y. Barbaux, Appl. Catal. A 199 (2000) 73.
[26] C.T. Krege, M.E. Leonowicz, W.J. Roth, J.C. Vartuli, J.S. Beck, Nature 359 (1992) 710.
[27] D. Trong On, D. Desplantier-Giscard, C. Danumach, D. Kaliaguine, Appl. Catal. A 222 (2001) 299.
[28] N. Ulagappon, C.N.R. Rao, Chem. Commun. (1996) 1047.
[29] W. Zhang, T.J. Pinnavaia, Catal. Lett. 38 (1996) 261.
[30] Z. Zhu, Z. Zhang, L. Kevan, J. Phys. Chem. B 103 (1999) 2680.
[31] J.S. Gonzalez, J.M. Robles, M.A. Rodriguez, P.M. Torres, E.R. Castellon, A.J. Lopez, Catal. Lett. 64 (2000) 209.
[32] D. Wei, N. Yao, G.L. Haller, Stud. Surf. Sci. Catal. 121 (1999) 239.
[33] T.K. Das, K. Chaudhari, E. Nandanan, A.J. Chandwakdar, A. Sudalai, T. Ravindranathan, S. Sivsanker, Tetrahedron Lett. 38 (1997) 3631.
[34] A. Sakthivel, P. Selvam, J. Catal. 211 (2002) 134.
[35] W.A. Carvallo, P.B. Varaldo, M. Wallau, U. Schuchardt, Zeolites 18 (1997) 408.
[36] R.A. Sheldon, M. Wallau, I.W.C.E. Arends, U. Schuchardt, Acc. Chem. Res. 31 (1998) 485.
[37] I.W.C.E. Arends, R.A. Sheldon, Appl. Catal. A 212 (2001) 175.
[38] X.Z. Zhang, Y.H. Yue, Z. Zao, Catal. Lett. 83 (2002) 19.
[39] Q. Zhang, Y. Wang, Y. Ohishi, T. Shishido, K. Takehira, J. Catal. 202 (2001) 308.
[40] Y. Wang, Q. Zhang, T. Shishido, K. Takehira, J. Catal. 209 (2002) 186.
[41] Q. Zhang, Y. Wang, S. Itsuki, T. Shishido, K. Takehira, J. Mol. Catal. A 188 (2002) 189.
[42] Y. Wang, Q. Zhang, Q. Guo, T. Chen, H. Wan, Y. Ohishi, T. Shishido, K. Takehira, Chem. Lett. 11 (2002) 1152.
[43] Y. Wang, Y. Ohishi, T. Shishido, Q. Zhang, W. Yang, Q. Guo, H. Wan, K. Takehira, J. Catal. 220 (2003) 347.
[44] D. Dollimore, G.R. Heal, J. Appl. Chem. 14 (1964) 109.
[45] K. Tanaka, H. Yamashita, R. Tsuchitani, T. Funabiki, T. Yoshida, J. Chem. Soc., Faraday Trans. 84 (1988) 2987.
[46] B.M. Weckhuysen, I.E. Wachs, R.A. Schoonheydt, Chem. Rev. 96 (1996) 3327.
[47] C. Pak, G.L. Haller, Micropor. Mesopor. Mater. 48 (2001) 165.
[48] J.-H. Choy, J.-B. Yoon, D.-K. Kim, S.-H. Hwang, Inorg. Chem. 34 (1995) 6524.
[49] D.J. Jones, J. Rozière, P. Maireras-Torres, A. Jiménez-López, P. Plivera-Pastor, E. Rodríguez-Castellón, A.A.G. Tomlinson, Inorg. Chem. 34 (1995) 4611.
[50] D.L. Hoang, H. Lieske, Thermochim. Acta 345 (2000) 93.
[51] K. Nakagawa, C. Kajita, K. Okumura, N. Ikenaga, M. Nishitani, T. Anpo, T. Kobayashi, T. Suzuki, J. Catal. 203 (2001) 87.
[52] K. Nakagawa, C. Kajita, Y. Ide, M. Okamura, S. Kato, H. Kasuya, N. Ikenaga, T. Kobayashi, T. Suzuki, Catal. Lett. 64 (2000) 215.
[53] Y. Sakurai, T. Suzaki, K. Nakagawa, N. Ikenaga, H. Aota, T. Suzuki, Chem. Lett. (2000) 526.
[54] Y. Sakurai, T. Suzaki, K. Nakagawa, N. Ikenaga, H. Aota, T. Suzuki, J. Catal. 209 (2002) 16.